

Geophysical Research Letters*



RESEARCH LETTER

10.1029/2024GL111115

Special Collection:

The U.S. GEOTRACES Pacific Meridional Transect (GP15)

Key Points:

- Enrichment of heavier Ni isotopes is observed in the surface ocean across the GP15 transect, particularly in the equatorial Pacific
- North Pacific deep ocean Ni isotope composition is nearly homogeneous and similar to previously reported values from other ocean basins
- Hydrothermal activity can both decrease and increase seawater Ni isotope composition, depending on vent geochemistry and proximity

Supporting Information:

Supporting Information may be found in the online version of this article.

Correspondence to:

X. Bian, xiaopenb@usc.edu

Citation:

Bian, X., Yang, S.-C., Raad, R. J., Odendahl, C. E., Lanning, N. T., Sieber, M., et al. (2024). Distribution and cycling of nickel and nickel isotopes in the Pacific Ocean. *Geophysical Research Letters*, 51, e2024GL111115. https://doi.org/10.1029/ 2024GL111115

Received 1 JUL 2024 Accepted 14 AUG 2024

Author Contributions:

Conceptualization: X. Bian,
J. N. Fitzsimmons, T. M. Conway,
S. G. John
Data curation: X. Bian, S.-C. Yang
Formal analysis: X. Bian, S.-C. Yang,
R. J. Raad
Funding acquisition: J. N. Fitzsimmons,
T. M. Conway, S. G. John
Investigation: X. Bian, S.-C. Yang,
R. J. Raad, C. E. Odendahl, N. T. Lanning,
M. Sieber

© 2024. The Author(s). This is an open access article under the terms of the Creative Commons Attribution License, which permits use, distribution and reproduction in any medium, provided the original work is properly cited.

Distribution and Cycling of Nickel and Nickel Isotopes in the Pacific Ocean

X. Bian¹, S.-C. Yang¹, R. J. Raad¹, C. E. Odendahl¹, N. T. Lanning², M. Sieber³, K.-F. Huang⁴, J. N. Fitzsimmons², T. M. Conway³, and S. G. John¹

¹Department of Earth Sciences, University of Southern California, Los Angeles, CA, USA, ²Department of Oceanography, Texas A&M University, College Station, TX, USA, ³College of Marine Science, University of South Florida, St Petersburg, FL, USA, ⁴Institute of Earth Sciences, Academia Sinica, Taipei, Taiwan

Abstract Nickel stable isotopes (δ^{60} Ni) provide insight to Ni biogeochemistry in the modern and past oceans. Here, we present the first Pacific Ocean high-resolution dissolved Ni concentration and δ^{60} Ni data, from the US GEOTRACES GP15 cruise. As in other ocean basins, increases in δ^{60} Ni toward the surface ocean are observed across the entire transect, reflecting preferential biological uptake of light Ni isotopes, however the observed magnitude of fractionation is larger in the tropical Pacific than the North Pacific Subtropical Gyre. Such surface ocean fractionation by phytoplankton should accumulate isotopically lighter Ni in the deep Pacific, yet we find that North Pacific deep ocean δ^{60} Ni is similar to previously reported values from the deep Atlantic. Finally, we find that seawater dissolved δ^{60} Ni in regions with hydrothermal input can be either higher or lower than background deep ocean δ^{60} Ni, depending on vent geochemistry and proximity.

Plain Language Summary A habitable Earth relies on the growth of microscopic plants, called phytoplankton, in the ocean. Phytoplankton help regulate Earth's climate and their growth requires various nutrients in seawater, including a suite of metal elements such as iron, zinc, and nickel (Ni). These metals are called trace metals in the ocean because their concentrations are extremely low in seawater, yet they are essential micronutrients. Therefore, it is important to understand how much and how these elements are supplied to and removed out of the ocean, and how they are used by phytoplankton. To study this question, we analyzed Ni isotope ratios of hundreds of seawater samples collected from the Pacific Ocean—which is the ratio of naturally occurring Ni atoms with different numbers of neutrons and therefore slightly different masses. We find that surface seawater is more enriched in heavier Ni isotopes than the deep seawater, in particular around the tropical Pacific. The deep ocean has similar Ni isotope ratios across different ocean basins, from the Atlantic to the Pacific. Seawater Ni isotope ratios are impacted by rivers near Alaska, submarine volcanos near Hawai'i, and a submarine volcanic chain called the East Pacific Rise.

1. Introduction

Nickel (Ni) is an important micronutrient for marine phytoplankton, serving as the cofactor for many essential enzymes that influence the global carbon and nitrogen cycles including superoxide dismutase, hydrogenase, and urease (Alfano & Cavazza, 2020; Ragsdale, 2009). Therefore, it is essential to study and understand Ni biogeochemistry in the modern ocean. Nickel stable isotopes (δ^{60} Ni) provide a powerful tool in Ni biogeochemical studies. Measurements of δ^{60} Ni for seawater and major Ni sources and sinks in the ocean have improved our understanding of the global ocean Ni isotope mass balance (Archer et al., 2020; Cameron & Vance, 2014; Ciscato et al., 2018; Fleischmann et al., 2023; Gall et al., 2013; Little et al., 2020; Revels et al., 2021; Vance et al., 2016). Analysis of seawater δ^{60} Ni may also provide insight into the internal cycling of Ni in the ocean, including such processes as biological uptake, regeneration, and scavenging. For example, δ^{60} Ni profiles in the oligotrophic ocean are characterized by heavier δ^{60} Ni (δ^{60} Ni $\approx +1.7\%$) in the surface seawater than in the deep ocean (δ^{60} Ni $\approx +1.3\%$), indicating preferential assimilation of lighter Ni isotopes by phytoplankton during biological uptake (Archer et al., 2020; Lemaitre et al., 2022; Takano et al., 2017; Yang et al., 2020).

Previous studies have reported seawater δ^{60} Ni from the Atlantic Ocean (Archer et al., 2020; Lemaitre et al., 2022), Southern Ocean (Wang et al., 2019), South Pacific (Takano et al., 2017), western North Pacific (Takano et al., 2022), and North Pacific upper ocean (Yang et al., 2020, 2021). However, data are particularly limited in the North Pacific, and have barely been reported for the deep North Pacific Ocean. Here, we present a high-resolution section of dissolved Ni concentrations and Ni isotopes from the US GEOTRACES Pacific Meridional Transect

BIAN ET AL. 1 of 10

Methodology: X. Bian, S.-C. Yang, R. J. Raad, C. E. Odendahl, S. G. John Resources: K.-F. Huang, T. M. Conway, S. G. John

Software: X. Bian, C. E. Odendahl, S. G. John

Supervision: S. G. John Validation: X. Bian, S.-C. Yang Visualization: X. Bian, C. E. Odendahl, S. G. John

Writing – original draft: X. Bian Writing – review & editing: X. Bian,

T. M. Conway, S. G. John

(GP15) cruise which sailed from the Alaskan margin (56°N) to Tahiti (20°S) along 152°W through the central Pacific, covering multiple oceanic regions with distinct biogeochemical features (Figure 1). Near the Alaskan continental margin, potential external Ni sources, such as rivers, may impact seawater Ni concentration and δ^{60} Ni. The oligotrophic North and South Pacific gyres provide the opportunity to study biologically driven Ni isotope fractionation in the surface ocean. The deep North Pacific, where the oldest seawater resides, is an important endmember for investigating the change in seawater δ^{60} Ni with deep ocean circulation. The GP15 transect also includes several regions where seawater is influenced by hydrothermal activity (Jenkins et al., 2020, 2023), providing an opportunity to explore the hydrothermal impact on seawater δ^{60} Ni. The high-resolution GP15 seawater Ni concentration and δ^{60} Ni data set presented here includes over 600 seawater dissolved Ni concentration and δ^{60} Ni observations, adding significantly to the global data set and providing insight to Ni biogeochemistry in the global ocean.

2. Materials and Methods

2.1. Seawater Sampling

Depth-profile and surface tow-fish seawater samples were collected aboard the R/V Roger Revelle (RR1814-RR1815) from the US GEOTRACES GP15 cruise. Hydrographic data including temperature, salinity, oxygen concentration, nutrient concentrations including phosphate, nitrate, and silicate, and seawater helium isotope ratios (δ^3 He) were taken from the publicly available data sets to provide context for Ni biogeochemistry (Casciotti et al., 2021a, 2021b; Jenkins & German, 2021a, 2021b).

Depth-profile seawater samples for Ni and δ^{60} Ni were collected using the GEOTRACES Trace-element Carousel sampling system (GTC) (Cutter et al., 2017, 2018). After collection, seawater was filtered from the GO-FLO bottles through Acropak capsules (0.2 μ m) into acid-washed 1 L LDPE bottles in the GEOTRACES trace-metal clean van. Surface samples were collected using a tow-fish sampling system (Cutter et al., 2018). Surface seawater was pumped up by a Teflon bellows pump and filtered by a 0.2 μ m filter cartridge into clean 1L LDPE bottles.

2.2. Nickel Concentration and Isotope Analysis

Seawater samples were acidified to pH \sim 1.8 by adding concentrated, distilled HCl (1 mL 12N HCl/1 L seawater) in a class 100 clean lab at the University of Southern California (USC). Meanwhile, 1 mL of 30% $\rm H_2O_2$ was also added to each 1 L seawater to destroy strong copper-binding ligands (Baconnais et al., 2019). Acidified samples were then stored for at least 6 months before Ni concentration and isotope analysis.

Dissolved Ni (dNi) concentrations were analyzed using a seaFAST-PicoTM offline system with an isotope dilution technique at USC and Texas A&M University (TAMU) (Hawco et al., 2020; Jensen et al., 2020). The USC dNi results are consistent with the TAMU dNi results (mean relative-difference is $-0.5 \pm 4.4\%$, 1SD, n = 762, Figure S1 in Supporting Information S1) and have been reported in John et al. (2022) for Ni biogeochemical modeling. For figures and discussions in this paper, we use the USC dNi results.

Seawater Ni isotope compositions were analyzed using a double-spike technique coupled with a prepFAST-MCTM offline system to purify Ni isotopes from seawater (Bian, Yang, Raad, Hawco, et al., 2024; Conway et al., 2013; Yang et al., 2020). The detailed procedure for sample purification and Ni isotope analysis is presented in Bian, Yang, Raad, Hawco, et al. (2024). Nickel isotopes were analyzed using a Thermo Neptune Plus multicollector ICP-MS (MC-ICP-MS) at USC, the University of South Florida (USF), and Academia Sinica (AS) and δ^{60} Ni results analyzed at USC, USF, and AS are consistent with each other (Figure S1 in Supporting Information S1). The double spike data reduction scheme followed the iterative method described by Siebert et al. (2001). The Ni isotope ratios were expressed using the delta notation relative to the NIST 986 Ni isotope standard:

$$\delta^{60} \text{Ni} = \left[\left(^{60} \text{Ni} \right)^{58} \text{Ni} \right)_{\text{sample}} / \left(^{60} \text{Ni} \right)^{58} \text{Ni} \right)_{\text{NIST 986}} - 1 \times 1000$$
 (1)

The accuracy of the method for seawater Ni isotope analysis has been previously demonstrated (Bian, Yang, Raad, Hawco, et al., 2024). The total procedural blank of Ni during sample processing is 0.33 ± 0.24 ng (2σ) , which is negligible for seawater δ^{60} Ni analysis. The analytical uncertainty of seawater δ^{60} Ni is 0.07%, consistent with repeated analysis of Ni isotope standards (Bian, Yang, Raad, Hawco, et al., 2024).

BIAN ET AL. 2 of 10

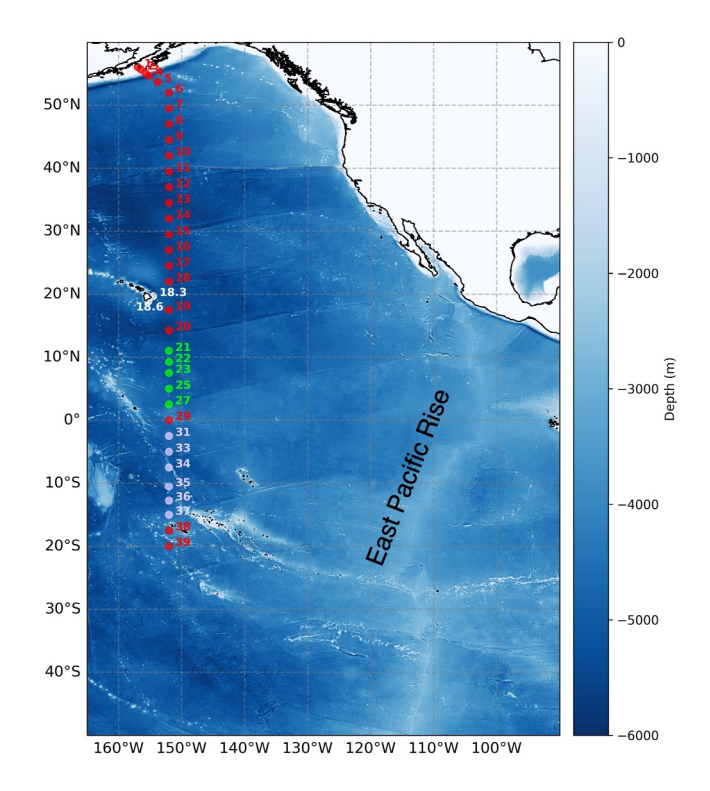


Figure 1. Track of the GP15 cruise in the Pacific Ocean. White dots denote the two stations (18.3 and 18.6) impacted by hydrothermal activity near Hawai'i. Green and light purple dots denote the stations where seawater δ^{60} Ni is potentially impacted by hydrothermal activity from the East Pacific Rise. The rest GP15 stations are represented as red dots, with corresponding station IDs labeled.

2.3. Nickel Isotope Modeling

A biogeochemical model of Ni isotope cycling in the global oceans provides context for our observations. This model was built in the AWESOME OCIM framework (John et al., 2020) and includes realistic three-dimensional ocean circulation, sources (river input) and sinks (burial of biogenic Ni into marine sediments) of Ni in the ocean, biological uptake of Ni by phytoplankton in the surface ocean with a Ni isotope fractionation factor, and regeneration of Ni in the deep ocean (without Ni isotope fractionation). Several model parameters were optimized to fit observations including the magnitude of Ni isotope fractionation during biological uptake, the remineralization length scale of sinking particulate Ni, and the isotope composition of riverine Ni input. A detailed description of the model is presented in Supporting Information S1.

3. Dissolved Ni Concentrations and $\delta^{60}\text{Ni}$ Across the GP15 Transect

Dissolved Ni has a nutrient-type distribution in the oceans; dissolved Ni concentrations are lower in the surface ocean compared to the deep, and increase from ~3 to 4 nmol/kg in the deep North Atlantic to ~10 nmol/kg in the deep North Pacific (Figures 2 and 4), related to water-mass mixing of preformed Ni and regeneration of additional Ni as water ages (John et al., 2022; Middag et al., 2020). In the surface of the oligotrophic gyres along GP15, where macronutrients are nearly completely depleted, dissolved Ni is drawn down to about 2 nmol/kg, but no lower (Figure 2 and Figure S2 in Supporting Information S1). In the subsurface nutricline, upwelling of Ni is observed in the tropical region (5°S and 10°N) as well as near the Alaskan margin. In the deep ocean, a Ni maximum is located at about 2,000 m, deeper than the phosphate and nitrate maxima, shallower than the silicate maximum (Figure 2 and Figure S2 in Supporting Information S1) (John et al., 2022).

The GP15 δ^{60} Ni section is characterized by higher δ^{60} Ni in the surface ocean (Figure 2). Above 500 m, seawater δ^{60} Ni values are mostly between +1.5 and +1.8%, compared to deep ocean values of +1.3 to +1.4%. Surface ocean δ^{60} Ni in the tropical Pacific (10°S to 10°N) is notably higher than the δ^{60} Ni in the North Pacific Subtropical Gyre (NPSG) at equivalent Ni concentrations. For example, surface seawater at Station 35 (above 50m, 10.5°S) has a mean dissolved Ni concentration of 2.51 \pm 0.08 nmol/kg (2SD, n=3) and δ^{60} Ni of +1.77 \pm 0.03% (2SD, n=3). In contrast, surface seawater (above 50 m) from the oligotrophic NPSG portion of GP15 (17.5–40°N) has an average dissolved Ni concentration of 2.40 \pm 0.40 nmol/kg (2SD, n=26) and δ^{60} Ni of +1.63 \pm 0.12% (2SD, n=17). Surface seawater at Station 35 thus has a similar Ni concentration but a δ^{60} Ni 0.14% higher than the NPSG, indicating greater Ni isotope fractionation in the tropical Pacific.

Below 1,000 m, seawater δ^{60} Ni is nearly homogeneous (mean of +1.34 \pm 0.11%, 2SD, n = 303). However, there are a few obvious regions with anomalous δ^{60} Ni compared to background, including low δ^{60} Ni (mean of +1.26 \pm 0.04%, 2SD, n = 4) near the Kama'ehuakanaloa (previously known as Lōʻihi) seamount, low δ^{60} Ni (mean of +1.24 \pm 0.01%, 2SD, n = 3) near the Puna Ridge seamount, and perhaps slightly elevated δ^{60} Ni associated with elevated δ^{3} He originating from the East Pacific Rise (Figure 2). Low surface δ^{60} Ni values are also observed near the Alaskan margin, with a mean of +1.29 \pm 0.07% (2SD, n = 7).

Deep ocean δ^{60} Ni from the GP15 section is similar to deep ocean δ^{60} Ni from other ocean basins. Mean GP15 δ^{60} Ni for waters below 1,000 m is +1.34 ± 0.11% (2SD, n=303) (Figure 2). Removing samples which may be impacted by hydrothermal inputs (Regions 1 to 4 in Figure 2, Section 4.4) yields a similar mean δ^{60} Ni of +1.33 ± 0.10% (2SD, n=254). This is similar to other ocean basins, including the North Atlantic (+1.36 ± 0.12%, 2SD, water depth >1,000 m; Lemaitre et al., 2022), the South Atlantic (+1.33 ± 0.13%, 2SD; Archer et al., 2020), the Indian sector of the Sothern Ocean (+1.33 ± 0.07%, 2SD, water depth >1,000 m; Wang et al., 2019), the South Pacific (+1.32 ± 0.03%, 2SD, water depth >2,000 m; Takano et al., 2017), and the Western North Pacific (+1.32 ± 0.03%, 2SD, water depth >1,000 m; Takano et al., 2022).

BIAN ET AL. 3 of 10

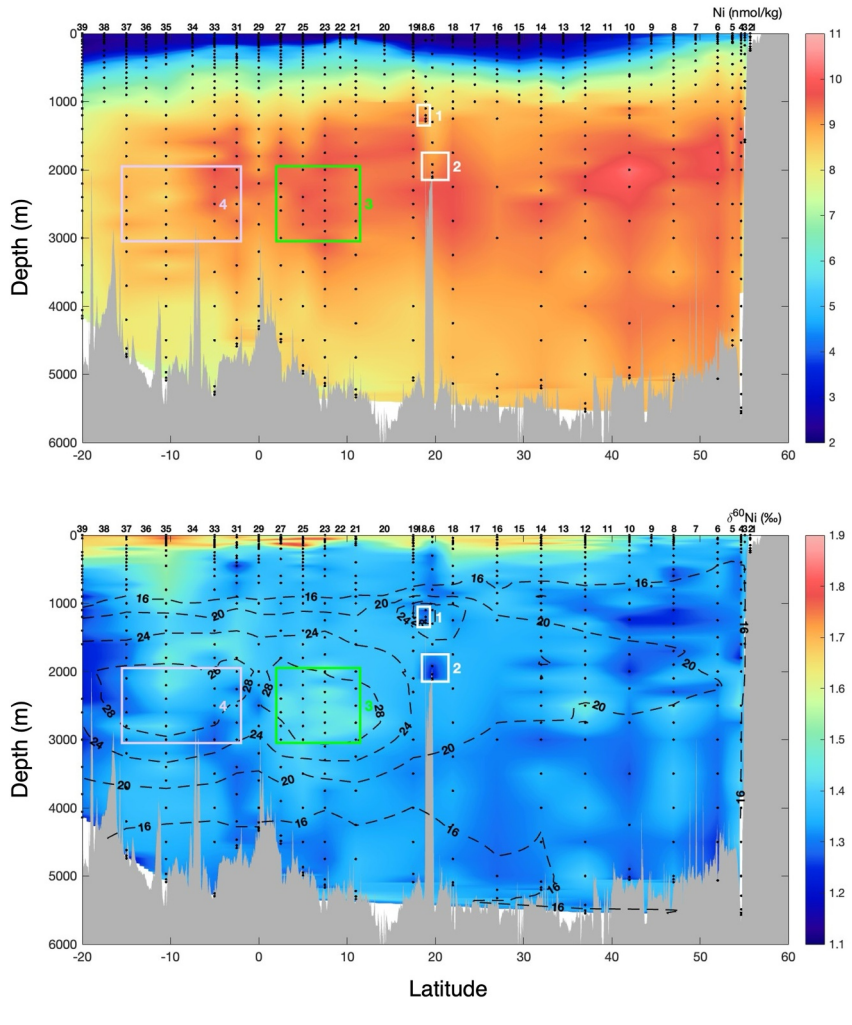


Figure 2. Sections of dissolved Ni and δ^{60} Ni along the GP15 transect. Station IDs are labeled above the section plots. The δ^{60} Ni section is overlaid with dashed contours of δ^3 He (%) with contour levels of 16, 20, 24, and 28 labeled. In both the Ni concentration and δ^{60} Ni sections, four regions where seawater δ^{60} Ni is potentially impacted by hydrothermal activity are highlighted by rectangles and labeled as 1, 2, 3, and 4 (1 and 2 represent the Kama'ehuakanaloa seamount and Puna Ridge, respectively; 3 and 4 represent the distal ends of the North and South East Pacific Rise, respectively).

4. Discussion

4.1. Fractionation of Ni Isotopes by Phytoplankton

Higher δ^{60} Ni and lower dissolved Ni concentrations in surface seawater have been well documented across diverse oceanic regions, particularly when Ni concentrations are below 4 nmol/kg (Figure 3; Archer et al., 2020; Lemaitre et al., 2022; Takano et al., 2017, 2022; Wang et al., 2019; Yang et al., 2020, 2021). This suggests preferential acquisition of lighter Ni isotopes during biological uptake. The abundant GP15 δ^{60} Ni data provide an excellent opportunity to investigate Ni isotope fractionation in the Pacific. Fitting the GP15 seawater δ^{60} Ni-[Ni] data set (above 200 m) to a closed-system Rayleigh distillation equation, we obtain a Ni isotope fractionation factor of $-0.30 \pm 0.05\%$ (2SE, $R^2 = 0.535$), with lighter Ni isotopes preferentially assimilated (Figure S4 in Supporting Information S1). This is similar to the seawater δ^{60} Ni-[Ni] relationship observed in other oceanic regions (Figure S4 in Supporting Information S1), where a Ni isotope fractionation factor of $-0.27 \pm 0.03\%$ (2SE, $R^2 = 0.643$) best fits the data. These results suggest a similar magnitude of biological Ni isotope fractionation across diverse marine habitats.

However, a close examination reveals unique Ni isotope fractionation in the tropical Pacific (10° S to 10° N) compared to global trends (Figures 2 and 3; Figure S4 in Supporting Information S1). Notably, δ^{60} Ni values at

BIAN ET AL. 4 of 10

19448007, 2024, 16, Downloaded from https://agupubs.onlinelibrary.wiley.com/doi/10.1029/2024GL111115 by Tim Conway - University Of South Florida

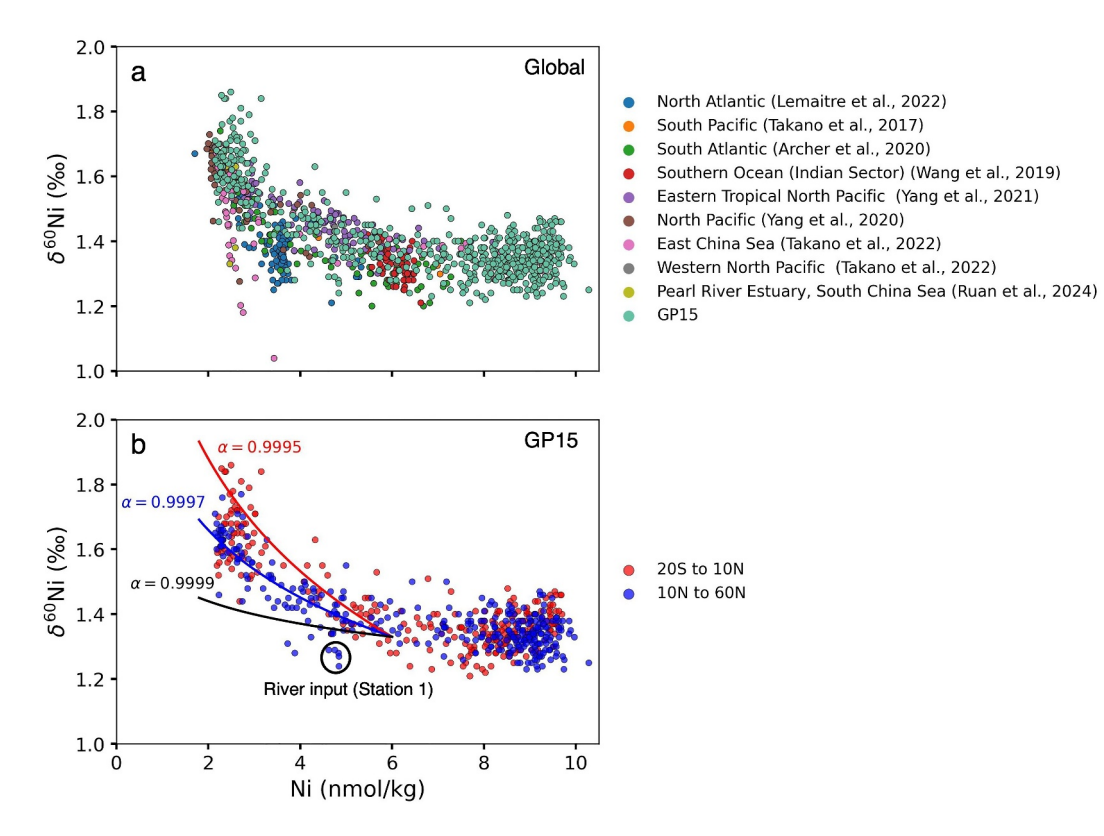


Figure 3. The relationship between dissolved Ni concentrations and δ^{60} Ni in the global ocean (a) and shown for GP15 samples north and south of 10° N (b). Three closed-system Rayleigh distillation curves are presented in panel (b), with a starting Ni concentration of 6 nmol/kg and three different Ni isotope fractionation factors representing fractionation during biological Ni uptake.

several GP15 stations in the equatorial Pacific are the highest yet reported (Section 3), indicating a larger isotope effect for Ni isotope fractionation in the tropical Pacific (Figure 3). The surface North Equatorial Current flows westward in the latitudinal range of about 8–18°N in the Pacific Ocean and serves as the southern boundary of the NPSG (Kessler, 2006; Liu & Zhou, 2020), such that 10°N is near the boundary that separates the NPSG from the tropical Pacific. The tropical Pacific and NPSG may have different microbial communities, or different environmental variables that lead to differences in Ni isotope fractionation even among similar species. It is notable that Ni is required for Ni superoxide dismutase (Ni-SOD) which protects phytoplankton from superoxide (O₂•¬) produced by UV radiation (C. Chen et al., 2022; L. Chen et al., 2022; Dupont et al., 2008; Ho, 2013; Ho et al., 2013; Rodriguez & Ho, 2014), and the tropical Pacific receives a higher solar radiation intensity than the NPSG. Laboratory culture studies of Ni isotope fractionation by phytoplankton are scarce (Cameron et al., 2009); but future work could help distinguish these hypotheses.

4.2. Homogeneous δ^{60} Ni in the Deep Ocean

The deep North Pacific has dissolved Ni concentrations about 2.5 times higher than the North Atlantic (3–4 vs. 8–10 nmol/kg) but similar δ^{60} Ni. This is inconsistent with expectations that lighter Ni isotopes should accumulate in older deep North Pacific waters. Assimilation of lighter Ni isotopes by phytoplankton in the surface ocean and remineralization of this biogenic Ni at depth should increase Ni concentrations and decrease δ^{60} Ni along the deep ocean "conveyor belt" from the North Atlantic to the North Pacific. This expectation is supported by the simple Ni isotope model we presented here (Section 2.3 and Figure 4), which nicely fits the Ni concentration data and predicts that seawater δ^{60} Ni in the deep North Pacific should be 0.05–0.1% lighter than the deep North Atlantic, at least when considering only preferential uptake of lighter Ni isotopes by phytoplankton in the surface ocean and regeneration of Ni at depth.

BIAN ET AL. 5 of 10

1029/2024GL111115 by Tim Conway

Wiley Online Library on [17/09/2024]. See the Ter

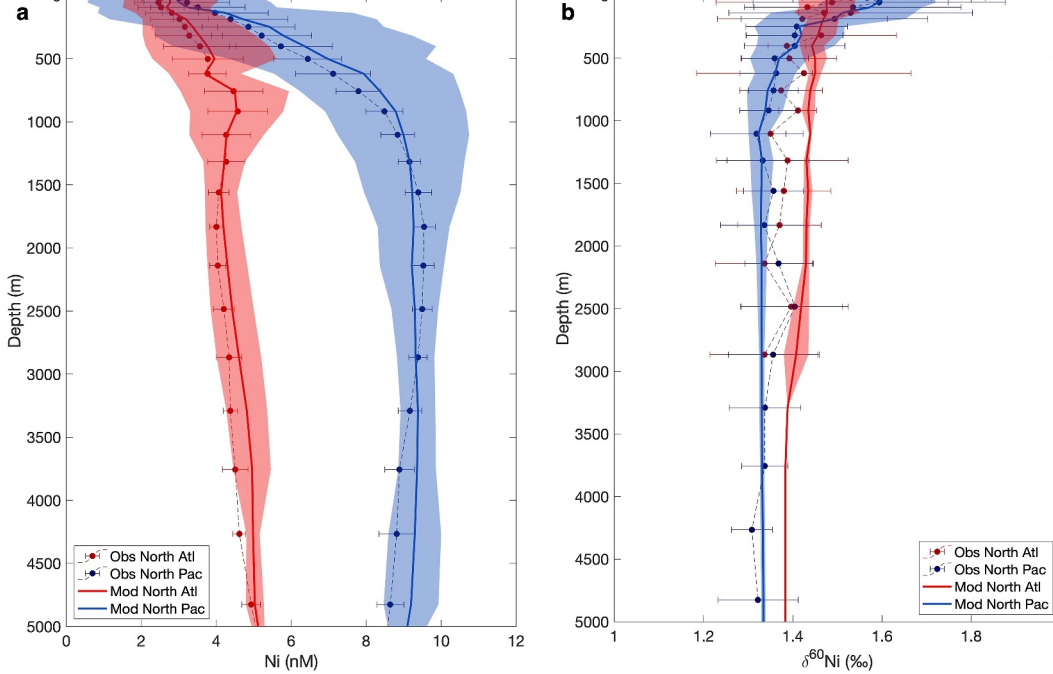


Figure 4. Comparison of model output with observations for dissolved Ni concentrations (a) and δ^{60} Ni (b) in the North Atlantic and North Pacific. Nickel concentration data include data from the GEOTRACES Intermediate Data Product 2021 (GEOTRACES Intermediate Data Product Group, 2021) and the GP15 cruise; global δ^{60} Ni data are the same as presented in Figure 3. Error bars of the observations are 2 standard deviations and shaded red and blue areas denote the 95% confidence intervals for the model predictions.

Processes not considered in the model, which may help to explain observations of homogeneous deep ocean δ^{60} Ni, include scavenging of Ni in the water column or a supply of heavy δ^{60} Ni from marine sediments. Scavenging of lighter Ni isotopes onto Mn oxides in the water column has been proposed to remove lighter Ni isotopes from seawater (Fleischmann et al., 2023), and models including reversible scavenging of Ni have been shown to produce a good fit to observations of Ni concentrations (John et al., 2022). A supply of isotopically heavy Ni from sediments has been previously hypothesized as a mechanism to achieve global ocean Ni isotope mass balance (Little et al., 2020), based on retention of lighter Ni isotopes in sediments during early diagenesis (Bian et al., 2023; Bruggmann et al., 2024; L. Chen et al., 2022; Little et al., 2020).

4.3. Riverine Ni Inputs Near the Alaskan Shelf

Riverine supply of Ni is observed in the GP15 transect near the Alaskan margin, especially at Station 1—the most nearshore station (Figures 2 and 3; Figure S5 in Supporting Information S1). Compared with Stations 2 and 3, surface seawater (above 40 m) at Station 1 has lower salinity (by 0.64 ± 0.28 psu, 1SD), higher dNi (by 0.36 ± 0.10 nmol/kg, 1SD), and lower δ^{60} Ni (by $0.12 \pm 0.03\%$, 1SD) (Figure S5 in Supporting Information S1). Low-salinity seawater from Station 1 does not follow the Ni- δ^{60} Ni relationship observed elsewhere throughout the global oceans (Figure 3), clearly indicating riverine input of isotopically lighter Ni to the ocean. This observation is consistent with other studies showing that river waters are generally isotopically lighter than seawater (Cameron & Vance, 2014; Revels et al., 2021; Ruan et al., 2024; Takano et al., 2022).

4.4. Impact of Hydrothermal Activity on Seawater δ^{60} Ni

The GP15 cruise also provided an excellent opportunity to investigate the impact of hydrothermal activity on Ni isotopes, both near venting sites (<100 km) and far field (>4,000 km). Three regions of the GP15 transect showed elevated ³He concentrations in seawater indicative of hydrothermal activity, one region near the Kama'ehuakanaloa seamount (Region 1 in Figure 2) and two regions between 2000 and 3,000 m near the equator representing the distal ends of North East Pacific Rise (NEPR, Region 3 in Figure 2) and South East Pacific Rise (SEPR,

BIAN ET AL. 6 of 10

Region 4 in Figure 2) (Jenkins et al., 2020, 2023; Lupton, 1998). A fourth region Puna Ridge near Hawai'i sampled waters impacted by a known submarine volcano, though ³He anomalies were not observed (Region 2 in Figure 2).

Previous studies have differed on whether hydrothermal fluids serve as a Ni source or a Ni sink in the ocean, and what impact this might have on ocean δ^{60} Ni. Hydrothermal fluids have a wide range of Ni concentrations depending on the nature of the hydrothermal venting (Diehl & Bach, 2020; Supporting Information S1). But much of the primary hydrothermal Ni can be scavenged onto Fe and Mn oxides in dilute plumes (Fitzsimmons et al., 2017; Fleischmann et al., 2023; Gueguen et al., 2021). It is also unclear whether hydrothermal vents are sources of isotopically light or isotopically heavy Ni to the oceans, since δ^{60} Ni of the mafic rocks from which hydrothermal fluids get Ni is much lighter than seawater (Elliott & Steele, 2017; Gall et al., 2017), but in dilute hydrothermal plumes lighter Ni isotopes may be preferentially removed from seawater, leaving heavier Ni isotopes behind (Fleischmann et al., 2023; Gueguen et al., 2021).

In the GP15 transect, a pronounced δ^3 He peak is observed at Station 18.6 between 1,100 and 1,300 m near the Kama'ehuakanaloa seamount (Region 1), indicating hydrothermal input. Within the δ^3 He peak (1,100–1,300 m; δ^3 He up to 400%, Figure S6 in Supporting Information S1), the average seawater dissolved Ni concentration at Station 18.6 is 0.86 nmol/kg higher than at the closest neighboring Station 18.3, and higher than at Stations 18 and 19. In addition, the average seawater δ^{60} Ni at Station 18.6 is 0.10% lighter than at Station 18.3, and lighter than at Stations 18 and 19 (Figure 2 and Figure S6 in Supporting Information S1). Previous studies have shown that dissolved Ni concentrations in Kama'ehuakanaloa hydrothermal fluids are up to 80 nmol/kg (Sedwick et al., 1992). Using seawater dissolved Ni concentration and δ^{60} Ni results from Stations 18.3 and 18.6, and assuming conservative mixing between hydrothermal fluids and seawater, we estimate the δ^{60} Ni of the hydrothermal end-member at Kama'ehuakanaloa would be $+0.63 \pm 0.74\%$ (2SE) (Figure S6 in Supporting Information S1). Even with this considerable uncertainty, it appears that the δ^{60} Ni of the Kama'ehuakanaloa endmember is significantly lower (p < 0.05) than the average deep seawater δ^{60} Ni of the GP15 transect $(+1.33 \pm 0.10\%)$. Lower seawater δ^{60} Ni values $(+1.24 \pm 0.01\%, 2SD, n = 3)$ are also observed near Puna Ridge (Region 2), although Ni concentration anomalies are not observed, which could be due either to a small input of Ni with a very low δ^{60} Ni, or an input of low- δ^{60} Ni hydrothermal fluids which is balanced by loss of pre-existing ocean dissolved Ni. These findings suggest that hydrothermal activity near Hawai'i supplies isotopically lighter Ni to the ocean. Whether these results can be generalized to other low-temperature hydrothermal systems, or other near-field hydrothermal environments, will require data from such regions elsewhere in the global ocean.

Seawater between 2000 and 3,000 m from Station 21 to Station 27 (11°N to 2.5°N, Region 3) represents the distal end of the NEPR as indicated by elevated δ^3 He. These waters have a mean δ^{60} Ni of $+1.42 \pm 0.06\%$ (2SD, n=24), which is 0.09% higher than the average deep seawater δ^{60} Ni across the entire transect GP15 transect (waters below 1,000 m, excluding hydrothermally influenced Regions 1–4; δ^{60} Ni = $+1.33 \pm 0.10\%$, n=254). A t-test shows that the difference is statistically significant (p < 0.001). Thus, seawater δ^{60} Ni in Region 3 may record the removal of isotopically light Ni within the NEPR hydrothermal plume. A hydrothermal impact on seawater δ^{60} Ni is less obvious in seawater influenced by the distal end of the SEPR (Station 31 to Station 37, 2,000–3,000 m from 2.5° S to 15° S, Region 4). Seawater in Region 4 has an average δ^{60} Ni of $+1.36 \pm 0.11\%$ (2SD, n=21), only 0.03% higher than the mean δ^{60} Ni of deep seawater unimpacted by hydrothermal activity ($+1.33 \pm 0.10\%$), and the difference has low statistical significance (p=0.09). The GP15 section is more than 5,000 km and 4,500 km away from the NEPR and the SEPR, respectively, and any hydrothermal impact we may observe is highly attenuated. While removal of isotopically light Ni in hydrothermal plumes has been previously inferred based on global Ni isotope mass balance and analysis of δ^{60} Ni in hydrothermally-impacted marine sediments (Fleischmann et al., 2023; Gueguen et al., 2021), our results provide the first direct seawater dissolved δ^{60} Ni evidence for this process.

5. Conclusions

This study presents the first high-resolution section of dissolved Ni concentration and δ^{60} Ni in the Pacific Ocean. The most striking feature observed in the surface ocean is elevated δ^{60} Ni, reflecting preferential uptake of lighter Ni isotopes by phytoplankton. Additionally, we observe a higher magnitude of Ni isotope fractionation in the equatorial Pacific compared to the NPSG. The preferential assimilation of lighter Ni isotopes into phytoplankton in surface oceans should lead to accumulation of lighter Ni isotopes in the older deep Pacific seawater, as

BIAN ET AL. 7 of 10

8 of 10



Acknowledgments

We thank all the scientists who

participated in the GEOTRACES GP15

cruise, particularly Laramie Jensen and

Brent Summers who assisted with sample

collection, as well as the captain and crew of the R/V Roger Revelle RR 1814–1815.

We thank Ethan Goddard for technical

assistance at USF. We thank Dr. Bleuenn

Guéguen and an anonymous reviewer for

Foundation awards OCE1736896 to SGJ.

OCE1737136 to TMC, OCE-1737167 to

JNF, and GRFP-1746932 to NTL, and the

Simons Foundation awards 426570SP and

their careful review. This study was

supported by the National Science

LI-SIAME-00001532 to SGJ.

BIAN ET AL.

Geophysical Research Letters

10.1029/2024GL111115

illustrated by a simple model of global ocean Ni biogeochemical cycling. However, we note a similar δ^{60} Ni in the deep oceans from the North Atlantic to the North Pacific. More complex models, for example, those that consider reversible scavenging of Ni and benthic sources of isotopically heavy Ni from marine sediments may be required to clarify the mechanisms leading to homogeneous deep ocean δ^{60} Ni.

We observed clear impacts from riverine input and hydrothermal activity on dissolved Ni concentration and δ^{60} Ni. Riverine input near the Alaskan margin supplies isotopically lighter Ni to the ocean. Hydrothermal activity impacts seawater δ^{60} Ni differently in different regions. Low-temperature hydrothermal fluids near the Kama'e-huakanaloa and Puna Ridge seamounts near Hawai'i supply isotopically light Ni to the ocean. In contrast, at locations distal to, but influenced by, high-temperature hydrothermal release from the NEPR, seawater δ^{60} Ni is higher than the background value, which may be attributed to the scavenging of lighter Ni isotopes by Fe-Mn oxides in the hydrothermal plume. This study provides early evidence from seawater δ^{60} Ni observations that hydrothermal activity can both decrease and increase seawater δ^{60} Ni, depending on the unique geochemistry of the hydrothermal vent and plume, and perhaps on proximity to the site of hydrothermal venting.

Data Availability Statement

Hydrographic data, nutrient concentrations, helium isotope ratios (δ^3 He), and dissolved Ni concentrations of GP15 seawater samples are publicly available from the Biological and Chemical Oceanography Data Management Office (BCO-DMO) (Bian et al., 2022a, 2022b; Casciotti et al., 2021a, 2021b; Jenkins & German, 2021a, 2021b). The GP15 dissolved Ni isotope data are publicly available on ResearchGate (Bian, Yang, Raad, Odendahl, et al., 2024).

References

- Alfano, M., & Cavazza, C. (2020). Structure, function, and biosynthesis of nickel-dependent enzymes. *Protein Science*, 29(5), 1071–1089. https://doi.org/10.1002/pro.3836
- Archer, C., Vance, D., Milne, A., & Lohan, M. C. (2020). The oceanic biogeochemistry of nickel and its isotopes: New data from the South Atlantic and the Southern Ocean biogeochemical divide. *Earth and Planetary Science Letters*, 535, 116118. https://doi.org/10.1016/j.epsl.
- Baconnais, I., Rouxel, O., Dulaquais, G., & Boye, M. (2019). Determination of the copper isotope composition of seawater revisited: A case study from the Mediterranean Sea. Chemical Geology, 511, 465–480. https://doi.org/10.1016/j.chemgeo.2018.09.009
- Bian, X., Yang, S.-C., Raad, R. J., Odendahl, C. E., Lanning, N., Sieber, M., et al. (2024). GEOTRACES GP15 seawater dissolved Ni and Ni isotope data [Dataset]. ResearchGate. https://doi.org/10.13140/RG.2.2.24034.75209
- Bian, X., Yang, S., & John, S. G. (2022a). Dissolved concentrations of nickel and copper from bottle samples collected on Leg 1 (Seattle, WA to Hilo, HI) of the US GEOTRACES Pacific Meridional Transect (PMT) cruise (GP15, RR1814) on R/V Roger Revelle from September to October 2018 (Version 1) [Dataset]. Biological and Chemical Oceanography Data Management Office (BCO-DMO). https://doi.org/10.26008/1912/bco-dmo.885319.1
- Bian, X., Yang, S., & John, S. G. (2022b). Dissolved concentrations of nickel and copper from bottle samples collected on Leg 2 (Hilo, HI to Papeete, French Polynesia) of the US GEOTRACES Pacific Meridional Transect (PMT) cruise (GP15, RR1815) on R/V Roger Revelle from October to November 2018 (Version 1) [Dataset]. Biological and Chemical Oceanography Data Management Office (BCO-DMO). https://doi.org/10.26008/1912/bco-dmo.885335.1
- Bian, X., Yang, S.-C., Raad, R. J., Hawco, N. J., Sakowski, J., Huang, K.-F., et al. (2024). A rapid procedure for isotopic purification of copper and nickel from seawater using an automated chromatography system. *Analytica Chimica Acta*, 1312, 342753. https://doi.org/10.1016/j.aca.2024. 342753
- Bian, X., Yang, S.-C., Raad, R. J., Lunstrum, A., Dong, S., Kemnitz, N., et al. (2023). Benthic flux of isotopically heavy Ni from sediments helps to resolve mass balance of nickel in the modern ocean. In *Presented at the Goldschmidt 2023 Conference*. GOLDSCHMIDT.
- Bruggmann, S., McManus, J., Archer, C., Vance, D., & Severmann, S. (2024). Nickel's behaviour in marine sediments under aerobic to anaerobic diagenetic conditions. Chemical Geology, 662, 122234. https://doi.org/10.1016/j.chemgeo.2024.122234
- Cameron, V., & Vance, D. (2014). Heavy nickel isotope compositions in rivers and the oceans. Geochimica et Cosmochimica Acta, 128, 195–211. https://doi.org/10.1016/j.gca.2013.12.007
- Cameron, V., Vance, D., Archer, C., & House, C. H. (2009). A biomarker based on the stable isotopes of nickel. Proceedings of the National Academy of Sciences, 106(27), 10944–10948. https://doi.org/10.1073/pnas.0900726106
- Casciotti, K. L., Cutter, G. A., & Lam, P. J. (2021a). Bottle file from Leg 1 (Seattle, WA to Hilo, HI) of the US GEOTRACES Pacific Meridional Transect (PMT) cruise (GP15, RR1814) on R/V Roger Revelle from September to October 2018 (Version 6) [Dataset]. Biological and Chemical Oceanography Data Management Office (BCO-DMO). https://doi.org/10.26008/1912/bco-dmo.777951.6
- Casciotti, K. L., Cutter, G. A., & Lam, P. J. (2021b). Bottle file from Leg 2 (Hilo, HI to Papeete, French Polynesia) of the US GEOTRACES Pacific Meridional Transect (PMT) cruise (GP15, RR1815) on R/V Roger Revelle from October to November 2018 (Version 5) [Dataset]. Biological and Chemical Oceanography Data Management Office (BCO-DMO). https://doi.org/10.26008/1912/bco-dmo.824867.5
- Chen, C., Rodriguez, I. B., Chen, Y. L., Zehr, J. P., Chen, Y., Hsu, S. D., et al. (2022). Nickel superoxide dismutase protects nitrogen fixation in *Trichodesmium. Limnology and Oceanography Letters*, 7(4), 363–371. https://doi.org/10.1002/lol2.10263
- Chen, L., Archer, C., Little, S. H., & Peacock, C. L. (2022). An isotopically heavy source of nickel: Release of nickel during birnessite transformation into todorokite. In *Presented at the 2022 Goldschmidt Conference*. GOLDSCHMIDT.
- Ciscato, E. R., Bontognali, T. R. R., & Vance, D. (2018). Nickel and its isotopes in organic-rich sediments: Implications for oceanic budgets and a potential record of ancient seawater. Earth and Planetary Science Letters, 494, 239–250. https://doi.org/10.1016/j.epsl.2018.04.061

4319/lo.2013.58.1.0112

- Conway, T. M. M., Rosenberg, A. D. A. D., Adkins, J. F. F., John, S. G., & John, J. G. (2013). A new method for precise determination of iron, zinc and cadmium stable isotope ratios in seawater by double-spike mass spectrometry. *Analytica Chimica Acta*, 793, 44–52. https://doi.org/10.1016/j.aca.2013.07.025
- Cutter, G. A., Casciotti, K., Croot, P., Geibert, W., Heimbürger, L.-E., Lohan, M. C., et al. (2017). Sampling and sample-handling protocols for GEOTRACES Cruises, Version 3.0.
- Cutter, G. A., Scientists, C.-C., Casciotti, K. L., & Lam, P. J. (2018). US GEOTRACES Pacific Meridional Transect—GP15 Cruise Report. Diehl, A., & Bach, W. (2020). MARHYS (MARine HYdrothermal Solutions) Database: A global Compilation of marine hydrothermal vent fluid, end member, and seawater compositions. Geochemistry, Geophysics, Geosystems, 21(12), e2020GC009385. https://doi.org/10.1029/
- Dupont, C. L., Barbeau, K., & Palenik, B. (2008). Ni uptake and limitation in marine Synechococcus strains. Applied and Environmental Microbiology, 74(1), 23–31. https://doi.org/10.1128/AEM.01007-07
- Elliott, T., & Steele, R. C. J. (2017). The isotope geochemistry of Ni. Reviews in Mineralogy and Geochemistry, 82(1), 511–542. https://doi.org/10.2138/rmg.2017.82.12
- Fitzsimmons, J. N., John, S. G., Marsay, C. M., Hoffman, C. L., Nicholas, S. L., Toner, B. M., et al. (2017). Iron persistence in a distal hydrothermal plume supported by dissolved–particulate exchange. *Nature Geoscience*, 10(3), 195–201. https://doi.org/10.1038/ngeo2900
- Fleischmann, S., Du, J., Chatterjee, A., McManus, J., Iyer, S. D., Amonkar, A., & Vance, D. (2023). The nickel output to abyssal pelagic manganese oxides: A balanced elemental and isotope budget for the oceans. *Earth and Planetary Science Letters*, 619, 118301. https://doi.org/ 10.1016/j.epsl.2023.118301
- Gall, L., Williams, H. M., Halliday, A. N., & Kerr, A. C. (2017). Nickel isotopic composition of the mantle. Geochimica et Cosmochimica Acta, 199, 196–209. https://doi.org/10.1016/j.gca.2016.11.016
- Gall, L., Williams, H. M., Siebert, C., Halliday, A. N., Herrington, R. J., & Hein, J. R. (2013). Nickel isotopic compositions of ferromanganese crusts and the constancy of deep ocean inputs and continental weathering effects over the Cenozoic. *Earth and Planetary Science Letters*, 375, 148–155. https://doi.org/10.1016/j.epsl.2013.05.019
- GEOTRACES Intermediate Data Product Group. (2021). The GEOTRACES Intermediate Data Product 2021 (IDP2021). NERC EDS British Oceanographic Data Centre NOC. https://doi.org/10.5285/cf2d9ba9-d51d-3b7c-e053-8486abc0f5fd
- Gueguen, B., Rouxel, O., & Fouquet, Y. (2021). Nickel isotopes and rare earth elements systematics in marine hydrogenetic and hydrothermal ferromanganese deposits. *Chemical Geology*, 560, 119999. https://doi.org/10.1016/j.chemgeo.2020.119999
- Hawco, N. J., Yang, S. C., Foreman, R. K., Funkey, C. P., Dugenne, M., White, A. E., et al. (2020). Metal isotope signatures from lava-seawater interaction during the 2018 eruption of Kīlauea. *Geochimica et Cosmochimica Acta*, 282, 340–356. https://doi.org/10.1016/j.gca.2020.05.005
 Ho, T. Y. (2013). Nickel limitation of nitrogen fixation in *Trichodesmium*. *Limnology and Oceanography*, 58(1), 112–120. https://doi.org/10.
- Ho, T. Y., Chu, T. H., & Hu, C. L. (2013). Interrelated influence of light and Ni on Trichodesmium growth. Frontiers in Microbiology, 4, 1–6. https://doi.org/10.3389/fmicb.2013.00139
- Jenkins, W. J., Doney, S. C., Seltzer, A. M., German, C. R., Lott, D. E., & Cahill, K. L. (2023). A North Pacific meridional section (U.S. GEOTRACES GP15) of helium isotopes and noble gases I: Deep water distributions. Global Biogeochemical Cycles, 37(5), e2022GB007667. https://doi.org/10.1029/2022GB007667
- Jenkins, W. J., & German, C. R. (2021a). Helium isotope with helium and neon concentration data from Leg 1 (Seattle, WA to Hilo, HI) of the US GEOTRACES Pacific Meridional Transect (PMT) cruise (GP15, RR1814) on R/V Roger Revelle from September to October 2018 (Version 1) [Dataset]. Biological and Chemical Oceanography Data Management Office (BCO-DMO). https://doi.org/10.26008/1912/bco-dmo.862182.1
- Jenkins, W. J., & German, C. R. (2021b). Helium isotope with helium and neon concentration data from Leg 2 (Hilo, HI to Papeete, French Polynesia) of the US GEOTRACES Pacific Meridional Transect (PMT) cruise (GP15, RR1815) on R/V Roger Revelle from Oct-Nov 2018 (Version 1) [Dataset]. Biological and Chemical Oceanography Data Management Office (BCO-DMO). https://doi.org/10.26008/1912/bco-dmo.862220.1
- Jenkins, W. J., Hatta, M., Fitzsimmons, J. N., Schlitzer, R., Lanning, N. T., Shiller, A., et al. (2020). An intermediate-depth source of hydrothermal ³He and dissolved iron in the North Pacific. *Earth and Planetary Science Letters*, 539, 116223. https://doi.org/10.1016/j.epsl.2020.116223
- Jensen, L. T., Wyatt, N. J., Landing, W. M., & Fitzsimmons, J. N. (2020). Assessment of the stability, sorption, and exchangeability of marine dissolved and colloidal metals. *Marine Chemistry*, 220, 103754. https://doi.org/10.1016/j.marchem.2020.103754
- John, S. G., Kelly, R. L., Bian, X., Fu, F., Smith, M. I., Lanning, N. T., et al. (2022). The biogeochemical balance of oceanic nickel cycling. *Nature Geoscience*, 15(11), 906–912. https://doi.org/10.1038/s41561-022-01045-7
- John, S. G., Liang, H., Weber, T., DeVries, T., Primeau, F., Moore, K., et al. (2020). AWESOME OCIM: A simple, flexible, and powerful tool for modeling elemental cycling in the oceans. Chemical Geology, 533, 119403. https://doi.org/10.1016/j.chemgeo.2019.119403
- Kessler, W. S. (2006). The circulation of the eastern tropical Pacific: A review. *Progress in Oceanography*, 69(2–4), 181–217. https://doi.org/10.1016/j.pocean.2006.03.009
- Lemaitre, N., Du, J., de Souza, G. F., Archer, C., & Vance, D. (2022). The essential bioactive role of nickel in the oceans: Evidence from nickel isotopes. *Earth and Planetary Science Letters*, 584, 117513. https://doi.org/10.1016/j.epsl.2022.117513
- Little, S. H., Archer, C., McManus, J., Najorka, J., Wegorzewski, A. V., & Vance, D. (2020). Towards balancing the oceanic Ni budget. Earth and Planetary Science Letters, 547, 116461. https://doi.org/10.1016/j.epsl.2020.116461
- Liu, X., & Zhou, H. (2020). Seasonal variations of the north equatorial current across the Pacific Ocean. *Journal of Geophysical Research: Oceans*, 125(6), e2019JC015895. https://doi.org/10.1029/2019JC015895
- Lupton, J. (1998). Hydrothermal helium plumes in the Pacific Ocean. Journal of Geophysical Research, 103(C8), 15853–15868. https://doi.org/10.1029/98JC00146
- Middag, R., de Baar, H. J. W., Bruland, K. W., & van Heuven, S. M. A. C. (2020). The distribution of nickel in the west-Atlantic Ocean, its relationship with phosphate and a comparison to cadmium and zinc. Frontiers in Marine Science, 7, 105. https://doi.org/10.3389/fmars.2020. 00105
- Ragsdale, S. W. (2009). Nickel-based enzyme systems. *Journal of Biological Chemistry*, 284(28), 18571–18575. https://doi.org/10.1074/jbc. R900020200
- Revels, B. N., Rickli, J., Moura, C. A. V., & Vance, D. (2021). Nickel and its isotopes in the Amazon Basin: The impact of the weathering regime and delivery to the oceans. *Geochimica et Cosmochimica Acta*, 293, 344–364. https://doi.org/10.1016/j.gca.2020.11.005
- Rodriguez, I. B., & Ho, T.-Y. (2014). Diel nitrogen fixation pattern of *Trichodesmium*: The interactive control of light and Ni. *Scientific Reports*, 4(1), 4445. https://doi.org/10.1038/srep04445

BIAN ET AL. 9 of 10

- Ruan, Y., Zhang, R., Yang, S.-C., Jiang, Z., Chen, S., Conway, T. M., et al. (2024). Iron, Nickel, Copper, Zinc, and their stable isotopes along a salinity gradient in the Pearl River Estuary, southeastern China. *Chemical Geology*, 645, 121893. https://doi.org/10.1016/j.chemgeo.2023.
- Sedwick, P. N., McMurtry, G. M., & Macdougall, J. D. (1992). Chemistry of hydrothermal solutions from Pele's Vents, Loihi Seamount, Hawaii. Geochimica et Cosmochimica Acta, 56(10), 3643–3667. https://doi.org/10.1016/0016-7037(92)90159-G
- Siebert, C., Nägler, T. F., & Kramers, J. D. (2001). Determination of molybdenum isotope fractionation by double-spike multicollector inductively coupled plasma mass spectrometry. *Geochemistry, Geophysics, Geosystems*, 2(7), 1032. https://doi.org/10.1029/2000GC000124
- Takano, S., Liao, W.-H., Ho, T.-Y., & Sohrin, Y. (2022). Isotopic evolution of dissolved Ni, Cu, and Zn along the Kuroshio through the East China Sea. *Marine Chemistry*, 243, 104135. https://doi.org/10.1016/j.marchem.2022.104135
- Takano, S., Tanimizu, M., Hirata, T., Shin, K. C., Fukami, Y., Suzuki, K., & Sohrin, Y. (2017). A simple and rapid method for isotopic analysis of nickel, copper, and zinc in seawater using chelating extraction and anion exchange. *Analytica Chimica Acta*, 967, 1–11. https://doi.org/10.1016/j.aca.2017.03.010
- Vance, D., Little, S. H., Archer, C., Cameron, V., Andersen, M. B., Rijkenberg, M. J. A., & Lyons, T. W. (2016). The oceanic budgets of nickel and zinc isotopes: The importance of sulfdic environments as illustrated by the Black Sea. *Philosophical Transactions of the Royal Society A: Mathematical, Physical & Engineering Sciences*, 374(2081), 20150294. https://doi.org/10.1098/rsta.2015.0294
- Wang, R.-M., Archer, C., Bowie, A. R., & Vance, D. (2019). Zinc and nickel isotopes in seawater from the Indian Sector of the Southern Ocean: The impact of natural iron fertilization versus Southern Ocean hydrography and biogeochemistry. Chemical Geology, 511, 452–464. https://doi.org/10.1016/j.chemgeo.2018.09.010
- Yang, S.-C., Hawco, N. J., Pinedo-González, P., Bian, X., Huang, K.-F., Zhang, R., & John, S. G. (2020). A new purification method for Ni and Cu stable isotopes in seawater provides evidence for widespread Ni isotope fractionation by phytoplankton in the North Pacific. Chemical Geology, 547, 119662. https://doi.org/10.1016/j.chemgeo.2020.119662
- Yang, S.-C., Kelly, R. L., Bian, X., Conway, T. M., Huang, K. F., Ho, T. Y., et al. (2021). Lack of redox cycling for nickel in the water column of the Eastern tropical north pacific oxygen deficient zone: Insight from dissolved and particulate nickel isotopes. *Geochimica et Cosmochimica Acta*, 309, 235–250. https://doi.org/10.1016/j.gca.2021.07.004

References From the Supporting Information

- Baumberger, T. (2011). Volatiles in marine hydrothermal systems.
- Binns, R. A., Scott, S. D., Bogdanov, Y. A., Lisitzin, A. P., Gordeev, V. V., Gurvich, E. G., et al. (1993). Hydrothermal oxide and gold-rich sulfate deposits of Franklin Seamount, western Woodlark Basin, Papua New Guinea. *Economic Geology*, 88(8), 2122–2153. https://doi.org/10.2113/
- DeVries, T. (2014). The oceanic anthropogenic CO₂ sink: Storage, air-sea fluxes, and transports over the industrial era. *Global Biogeochemical Cycles*, 28(7), 631–647. https://doi.org/10.1002/2013GB004739
- Diehl, A., & Bach, W. (2023). MARHYS Database 3.0 [Dataset]. PANGAEA. https://doi.org/10.1594/PANGAEA.958978
- Douville, E., Charlou, J. L., Oelkers, E. H., Bienvenu, P., Colon, C. F. J., Donval, J. P., et al. (2002). The rainbow vent fluids (36°14VN, MAR): The influence of ultramafic rocks and phase separation on trace metal content in Mid-Atlantic Ridge hydrothermal fluids. *Chemical Geology*, 184(1–2), 37–48. https://doi.org/10.1016/s0009-2541(01)00351-5
- Evans, G. N., Seyfried, W. E., & Tan, C. (2023). Nutrient transition metals in a time series of hydrothermal vent fluids from Main Endeavour Field, Juan de Fuca Ridge, Pacific Ocean. Earth and Planetary Science Letters, 602, 117943. https://doi.org/10.1016/j.epsl.2022.117943
- Gueguen, B., Sorensen, J. V., Lalonde, S. V., Peña, J., Toner, B. M., & Rouxel, O. (2018). Variable Ni isotope fractionation between Fe-oxyhydroxides and implications for the use of Ni isotopes as geochemical tracers. *Chemical Geology*, 481, 38–52. https://doi.org/10.1016/j.chemgeo.2018.01.023
- Liang, H., Moffett, J. W., & John, S. G. (2023). Toward a better understanding of the global ocean copper distribution and speciation through a data-constrained model. Global Biogeochemical Cycles, 37(9), e2023GB007769. https://doi.org/10.1029/2023GB007769
- Marques, A. F. A., Roerdink, D. L., Baumberger, T., De Ronde, C. E. J., Ditchburn, R. G., Denny, A., et al. (2020). The Seven Sisters hydrothermal system: First record of shallow hybrid mineralization hosted in mafic volcaniclasts on the Arctic mid-ocean ridge. *Minerals*, 10(5), 439. https://doi.org/10.3390/min10050439
- Schmidt, K., Garbe-Schönberg, D., Hannington, M. D., Anderson, M. O., Bühring, B., Haase, K., et al. (2017). Boiling vapour-type fluids from the Nifonea vent field (New Hebrides Back-Arc, Vanuatu, SW Pacific): Geochemistry of an early-stage, post-eruptive hydrothermal system. Geochimica et Cosmochimica Acta, 207, 185–209. https://doi.org/10.1016/j.gca.2017.03.016
- Seewald, J., Cruse, A., & Saccocia, P. (2003). Aqueous volatiles in hydrothermal fluids from the Main Endeavour Field, northern Juan de Fuca Ridge: Temporal variability following earthquake activity. *Earth and Planetary Science Letters*, 216(4), 575–590. https://doi.org/10.1016/S0012-821X(03)00543-0
- Seyfried, W. E., Seewald, J. S., Berndt, M. E., Ding, K., & Foustoukos, D. I. (2003). Chemistry of hydrothermal vent fluids from the Main Endeavour Field, northern Juan de Fuca Ridge: Geochemical controls in the aftermath of June 1999 seismic events. *Journal of Geophysical Research*, 108(B9), 2002JB001957. https://doi.org/10.1029/2002JB001957
- Sorensen, J. V., Gueguen, B., Stewart, B. D., Peña, J., Rouxel, O., & Toner, B. M. (2020). Large nickel isotope fractionation caused by surface complexation reactions with hexagonal birnessite. *Chemical Geology*, 537, 119481. https://doi.org/10.1016/j.chemgeo.2020.119481
- Wang, S.-J., & Wasylenki, L. E. (2017). Experimental constraints on reconstruction of Archean seawater Ni isotopic composition from banded iron formations. Geochimica et Cosmochimica Acta, 206, 137–150. https://doi.org/10.1016/j.gca.2017.02.023
- Wasylenki, L. E., Howe, H. D., Spivak-Birndorf, L. J., & Bish, D. L. (2015). Ni isotope fractionation during sorption to ferrihydrite: Implications for Ni in banded iron formations. *Chemical Geology*, 400, 56–64. https://doi.org/10.1016/j.chemgeo.2015.02.007
- Wheat, C. G., Mottl, M. J., & Rudnicki, M. (2002). Trace element and REE composition of a low-temperature ridge-flank hydrothermal spring. Geochimica et Cosmochimica Acta, 66(21), 3693–3705. https://doi.org/10.1016/S0016-7037(02)00894-3
- Wheat, C. G., Jannasch, H. W., Kastner, M., Plant, J. N., & DeCarlo, E. H. (2003). Seawater transport and reaction in upper oceanic basaltic basement: Chemical data from continuous monitoring of sealed boreholes in a ridge flank environment. *Earth and Planetary Science Letters*, 216(4), 549–564. https://doi.org/10.1016/S0012-821X(03)00549-1

BIAN ET AL. 10 of 10